Hindawi Publishing Corporation
Shock and Vibration
Volume 2015, Article ID 863961, 11 pages
http://dx.doi.org/10.1155/2015/863961

Research Article

Settlement Behaviors of Metro Tunnels during the Metro Operation

Wenbo Shi,[1] Linchang Miao,[1] Zhengxing Wang,[2] and Junhui Luo[1]

[1]*Institute of Geotechnical Engineering, Southeast University, Nanjing 210018, China*
[2]*Urban and Rural Construction Bureau, Nantong 226000, China*

Correspondence should be addressed to Linchang Miao; lc.miao@seu.edu.cn

Received 5 May 2015; Revised 4 August 2015; Accepted 12 August 2015

Academic Editor: Salvatore Strano

Copyright © 2015 Wenbo Shi et al. This is an open access article distributed under the Creative Commons Attribution License, which permits unrestricted use, distribution, and reproduction in any medium, provided the original work is properly cited.

This paper investigates the settlement behaviors of a metro tunnel during metro operation. A nonlinear vibration model of vehicle-track is established, and a series of vibration loadings for the frequency domain acting on segments are obtained based on a modal analysis method and applying the Fourier transformation algorithm. The displacements at any position in the soil are derived from the segment-soil interaction coupled model with the elastic continuum theory, and its accuracy is verified by comparing with the calculation result obtained by elastic-plastic finite element model.

1. Introduction

With the sustained development of urbanization, the population of major cities continues to expand at unprecedented rates. The traffic congestion in cities has become a "bottleneck," restricting the economic development of cities and affecting the travel of the residents of cities. The metro, a fast, convenient, and environment-friendly transportation network, has been rapidly constructed in a growing number of cities. However, the vertical displacement of the metro tunnel is induced by the vibration of the train, substantially influencing the operational safety of the metro. This subsidence has approached 30 cm between the People's Square Station and the Hanzhong Road Station of metro Line 1 in Shanghai from 1995 to 2015, and the largest subsidence near the Hailun Road Station of metro Line 4 in Shanghai has reached 16 cm [1]. Therefore, the settlement features of metro tunnels under vehicle-track vibration action must be analyzed.

In previous studies, many researchers considered that excitation model of vehicle-track vibration is independent of a segment-soil interaction coupled model and the two models had been studied, respectively. This way can be convenient to study the effect of metro train vibration, but the vehicle-track dynamic features cannot illustrate the settlement effect of metro tunnel caused by the metro train vibration directly. Multiple studies on vehicle-track dynamics have been performed by establishing the coupling model. Timoshenko [2] firstly proposed the frequency domain technique to analyze track dynamics for a continuously supported Euler beam. Dieterman and Metrikine [3] used a model of a point harmonic load moving along an elastic layer resting on a rigid foundation to study the critical speeds in the ballast layer. Caughey and O'Kelly [4] analyzed the influence of the damping coefficients of the vehicle on the natural frequency of the system. Garvey et al. [5] introduced a new type of coordinate conversion method to solve the equations for a vehicle-track system. In recent studies, vehicle and track models have been considered as an integral system in the dynamics of wheel-rail interactions [6–12].

The propagation features of vibration caused by the wheel-rail dynamic system in the ground have also been developed. Hunt [13] presented a simplified analytical method to calculate the ground vibration propagation from metros with tunnel and building models of infinite length. Balendra et al. [14] created a cross-sectional tunnel model embedded in a viscoelastic half-space based on the two-dimensional (2D) wave equation. Krylov and Ferguson [15] construed each sleeper under the metro track as a point load by assuming the tunnel diameter to be smaller than the wavelength of low-frequency propagated waves. Forrest and

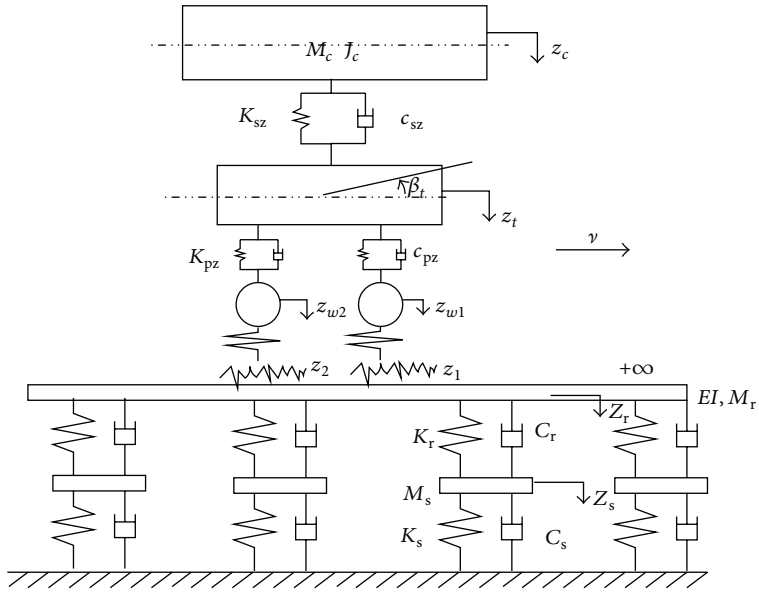

Figure 1: The vehicle-track coupled nonlinear model.

Hunt [16] described an analytical three-dimensional model for the dynamics of a deep underground railway tunnel in infinite soil to analyze the ground vibration because of the excitation by running trains in frequencies of 20 to 100 Hz. Metrikine and Vrouwenvelder [17] established a modular model consisting of static deflection model, track model, and the propagation model, and the effect of changing element size, soil stiffness, damping, and boundary conditions is analyzed. Gardien and Stuit [18] described in detail the mesh refinement and coarsening in the case of HST applications, with successful validations. Ekevid et al. [19] investigate the characteristics of building vibrations induced by adjacent moving trucks using finite element analyses. Regarding urban traffic, research is scarcer. Ju [20] studied the effect of ground-borne vibrations generated by underground metro and their effects on ancient monuments. Many additional studies have been performed on the generation and propagation of stress waves in an elastic medium containing a cavity because of an arbitrary dynamic loading applied on the cavity [21–24].

However, the settlement of the tunnel during the metro operation calculated by vehicle-track coupling model and tunnel-soil coupling model is also rare. This paper predicts the displacement of the tunnel under the exciting action of vehicle-track vibration. The calculation results show that this research can be a tool for engineers to use when designing metro tunnels embedded in soft soil areas.

2. Excitation Model for Vehicle-Track Vibration

The settlement of the soil surrounding the metro tunnel results from vehicle-tract vibration during operation. The magnitude of the settlement is mainly affected by the force on the vehicle-track contact surface, the vibration frequency, and the vertical vibration acceleration of the system. Controlling metro train vibration becomes an essential key technique to reduce the soil settlement surrounding the metro tunnel. For a thorough investigation of the behaviors of the different track components, a detailed description of the dynamical features of the track structure is required. The heaving vibration of a car body with nodding vibration will not cause coupling. Therefore, the half car body model based on the characteristics of an elastic supporting block ballast-less track is established as shown in Figure 1.

2.1. Establishing the Vehicle Model. As shown in Figure 1, the symbols M_c, M_t, and M_w indicate the mass of the train body, the bogie, and the wheel set, respectively; J_t is the nod inertia of the frame of the body; K_{sz} and K_{pz} are the stiffness of the primary and secondary suspensions of the vehicle, respectively; C_{sz} and C_{pz} are the damping of the primary and secondary suspensions of the vehicle, respectively; z_1 and z_2 are the location of the wheel-rail contact. The vibration equation of the vehicle model is established according to the Hamilton principle as follows:

$$[M_u]\{\ddot{u}\} + [C_u]\{\dot{u}\} + [K_u]\{u\} = \{P_u\}, \quad (1)$$

where P_u is the force at the wheel-rail contact position and u is the displacement vector of the train system.

2.2. Establishing the Track Model. The elastic supporting block ballast-less track is supported by the rail, fasteners, concrete supporting block, and rubber pads under the supporting block, rubber boots, and concrete track bed. The vertical stiffness and damping of the track are mainly provided by the fasteners and the rubber pad. In the model, these can be expressed as K_r and C_r or K_s and C_s, respectively. Additionally, the acceleration of the vibration in the elastic supporting block ballast-less track is mainly reflected in the rail and concrete supporting block.

Newton and Clark [25] analyzed the effect of the vehicle-track coupling nonlinear system assuming the track as an Euler beam and Timoshenko beam. The results showed that the Timoshenko beam has a higher accuracy analyzing the rail shear stress and bending deformation; however, the computational time was higher for the Timoshenko beam. This paper uses the Euler model because the two beams have little difference in accuracy in the analysis of the vertical vibration displacement of the track. The equation for the rail vibration deformation is established as follows:

$$EI\frac{\partial^4 Z_{\mathrm{r}}(x,t)}{\partial x^4} + m_{\mathrm{r}}\frac{\partial^2 Z_{\mathrm{r}}(x,t)}{\partial t^2} = -\sum_{i=1}^{N} F_{\mathrm{rs}i}(t)\,\delta(x - x_i) + \sum_{j=1}^{2} p_j(t)\,\delta\left(x - x_{wj}\right), \tag{2}$$

where $F_{\mathrm{rs}i}(t) = K_{\mathrm{r}i}[Z_{\mathrm{r}}(x_i,t) - Z_{si}(t)] + C_{\mathrm{r}i}[\dot{Z}_{\mathrm{r}}(x_i,t) - \dot{Z}_{si}(t)]$, δ is the Dirac function, $Z_{si}(t)$ is the sleeper vibration displacement, $F_{\mathrm{rs}i}$ is the reaction for the ith root sleeper, and p_j is the wheel-rail coupling force at the sites of the jth wheels.

The vibration equation on sleeper is as follows:

$$K_{\mathrm{r}}\left[Z_{\mathrm{r}}(x_i,t) - Z_{\mathrm{s}i}(t)\right] + C_{\mathrm{r}}\left[\dot{Z}_{\mathrm{r}}(x_i,t) - \dot{Z}_{\mathrm{s}i}(t)\right] - K_{\mathrm{s}}Z_{\mathrm{s}i}(t) - C_{\mathrm{s}}\dot{Z}_{\mathrm{s}i}(t) = M_{\mathrm{s}i}\ddot{Z}_{\mathrm{s}i}(t). \tag{3}$$

The two ends of the rail are assumed to be simply supported. Therefore, the boundary conditions for the moment can be obtained: the displacement of the rail and bending moment on the cross section are zero at $x = 0$ [26, 27].

The corresponding characteristic function, namely, the free vibration modal, is as follows:

$$Y_r(x) = C_1 \sin\frac{r\pi x}{l} \quad (r = 1, 2, \ldots). \tag{4}$$

Orthogonal processing of the characteristics function using $\int_0^L mY_r^2(x)dx = 1$ results in $C_1 = \sqrt{2/ml}$. Therefore, the free vibration modal equation is as follows:

$$Y_r(x) = \sqrt{\frac{2}{ml}} \sin\frac{r\pi x}{l} \quad (r = 1, 2, \ldots). \tag{5}$$

Therefore,

$$Z_r(x_i,t) = Y(x)\,q(t) = \sqrt{\frac{2}{m_r l}} \sin\frac{k\pi x}{l} q_k(t). \tag{6}$$

Simplifying the track nonlinearity equations by substituting (6) into (2) and (3) results in the final vibration equation:

$$[M_1]\{\ddot{q}\} + [C_1]\{\dot{q}\} + [K_1]\{q\} = \{P_1\}, \tag{7}$$

where q is the displacement vector of the track system.

A sufficient mode number guarantees the precision in the process of solving the vibration equation for the track using the modal analysis method [28]. According to the results of numerical modeling, the calculation accuracy can satisfy the requirements when the mode number exceeds $0.5L/L_{\mathrm{s}}$, where L is the rail length and L_{s} is the distance of the adjacent sleepers.

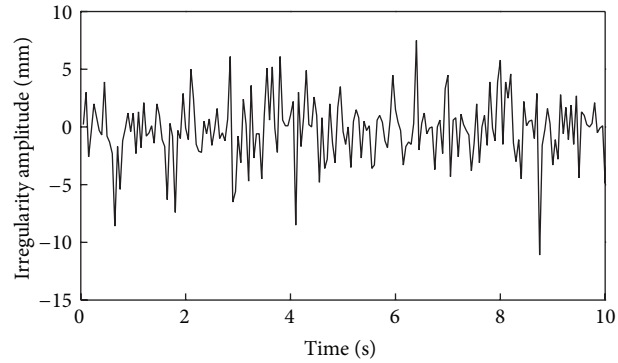

Figure 2: Track random irregularity.

2.3. Calculating the Contact Stress of the Wheel Track. The calculation for the wheel-track contact stress can become true by the Hertz nonlinear contact theory; therefore, the wheel-track vertical force is as follows:

$$p(t) = \left[\frac{1}{G}\delta_{Z(t)}\right]^{3/2}, \tag{8}$$

where G is the wheel-rail contact constant (the wheel-rail contact empirical formula for a contact constant is $G = 4.57R^{-0.149} \times 10^{-8}$), $\delta_{Z(t)}$ indicates the elastic compression between the wheel and track, and R is the radius of the wheel.

Connecting the vehicle model to the lower track model produces an integrated system when using (8).

2.4. Applying the Random Irregular Model. The rail surface geometry is influenced by many complex factors such as irregularity cracks, fissures, crevasses, and smoothness. The effects caused by track irregularity display randomness. The most realistic representation in vehicle-track modeling is to describe the travel of the vehicle over the irregularity and to denote the nondeterministic excitation in the wheel-track system as a stochastic irregularity. The calculation uses the spectrum density function of the metro track for grade six lines from the America Railway Standard. A simulation using a trigonometric series method converts the track irregularity power spectrum to the time domain excitation function, which is applied to the system as a random excitation. The final amplitude curves of the vertical track irregularity are shown in Figure 2.

2.5. The Newmark Integration Method. Time stepping integration provides the best method to achieve a numerical solution for the equations of motion of a vehicle-track system, which includes nonlinearities. The vehicle vibration equation and the track vibration equation are identical as shown in

$$[M]\{\ddot{x}\} + [C]\{\dot{x}\} + [K]\{x\} = \{P\}. \tag{9}$$

Implicit integration schemes may cause large amount of calculation because a large linear algebraic equation needed to be solved from integration; the cost is quite considerable. People search for Newmark explicit iterative method in view of this. Newmark explicit iterative method has the

characteristics with simple calculation process and high efficiency but needs to sacrifice certain precision and stability of the expense; meanwhile, the selection of time steps is limited to the stability. This paper uses a new forecast-revise integration method proposed by Zhai [29] on the basis of this. The method constructs an explicit integration form symmetrically through leading in two integral parameters φ and ψ. At the beginning of the form, set $\varphi = \psi = 0$; the forecast displacement and velocity are calculated using the following formula:

$$\begin{aligned}\{x\}_{p,n+1} &= \{x\}_n + \{\dot{x}\}_n \Delta t + \left(\frac{1}{2} + \psi\right) \{\ddot{x}\}_n \Delta t^2 \\ &\quad - \psi \{\ddot{x}\}_{n-1} \Delta t^2, \\ \{\dot{x}\}_{p,n+1} &= \{\dot{x}\}_n + (1 + \varphi) \{\ddot{x}\}_n \Delta t - \varphi \{\ddot{x}\}_{n-1} \Delta t.\end{aligned} \tag{10}$$

The forecast acceleration is obtained through

$$\begin{aligned}&\{\ddot{x}\}_{p,n+1} \\ &= [M]^{-1} \left(\{P\}_{n+1} - [K]_{n+1} \{x\}_{p,n+1} - [C]_{n+1} \{\ddot{x}\}_{p,n+1}\right).\end{aligned} \tag{11}$$

Substitute the forecast acceleration into revise integration equation:

$$\begin{aligned}\{x\}_{n+1} &= \{x\}_n + \{\dot{x}\}_n \Delta t + \left(\frac{1}{2} - \beta\right) \{\ddot{x}\}_n \Delta t^2 \\ &\quad + \beta \{\ddot{x}\}_{p,n+1} \Delta t^2 \\ \{\dot{x}\}_{n+1} &= \{\dot{x}\}_n + (1 - \gamma) \{\ddot{x}\}_n \Delta t + \gamma \{\ddot{x}\}_{p,n+1} \Delta t.\end{aligned} \tag{12}$$

And the accurate acceleration is got from

$$\begin{aligned}&\{\ddot{x}\}_{n+1} \\ &= [M]^{-1} \left(\{P\}_{n+1} - [K]_{n+1} \{x\}_{n+1} - [C]_{n+1} \{\ddot{x}\}_{n+1}\right).\end{aligned} \tag{13}$$

The results are similar to implicit integration schemes when time step length is 0.0001 s by large calculation.

For each time step, the responses of the displacements and velocities in the vehicle model and the track model are determined, and the nonlinear wheel-track contact forces can then be determined based on the calculated displacements and velocities. From these results, the acceleration of the vehicle and the track is calculated from the equations of motion.

3. Segment-Soil Interaction Coupled Model

Combined with the observation that two-dimensional modeling results are qualitatively in agreement with those of three-dimensional modeling at low frequencies, two-dimensional modeling required less computational effort [30]. The two-dimensional segment-soil interaction coupled model and a two-dimensional elastic continuum model are established in this section.

Jin [31, 32] presented a semianalytical treatment of a 2D half-plane porous media subjected to a surface-moving line load and the dynamic response of an infinite beam bonded to a half-space porous medium when subjected to a moving load. Metrikine studied the vibration of a surface of a two-dimensional (2D) elastic layer generated by a point load moving uniformly along a beam [17]. Rajapakse studied the modeling of a circular borehole embedded in a poroelastic medium subjected to a static ring load [33]. The settlement of the tunnel is calculated through establishing 2D numerical model with reference to the calculation model of infinite soil comprising a thin cylindrical shell composed by Forrest [16].

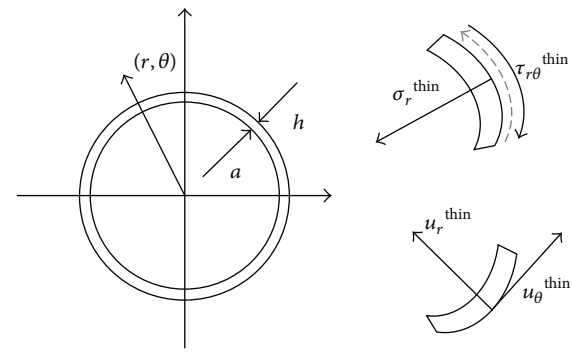

Figure 3: A thin-shell circle computing model.

3.1. Modeling Segment-Soil Interactions with the Elastic Continuum Theory. During the calculation, tunnel segments are assumed to be a thin-shell circle, and the material of the circle is liner-elastic, isotropic, and homogeneous. The main contribution of this study is the analysis of the vertical displacement of the metro tunnel during operation. The simplified computing model is shown in Figure 3, and (14) and (15) express the dynamic equilibrium in the two main directions.

Equilibrium in the radial direction provides the following:

$$\begin{aligned}&\frac{1}{a}\frac{\partial u_\theta^{\text{thin}}}{\partial \theta} - \frac{1}{a} u_r^{\text{thin}} - \frac{h^2}{12a^3}\frac{\partial^4 u_r^{\text{thin}}}{\partial \theta^4} \\ &\quad - \frac{h^2}{12}\left[\frac{1}{a^3} u_r^{\text{thin}} + \frac{2}{a^3}\frac{\partial^2 u_r^{\text{thin}}}{\partial \theta^2}\right] \\ &\quad + a\frac{\left(1 - \nu^2\right)}{Eh}\sigma_r^{\text{thin}} - \rho a \frac{\left(1 - \nu^2\right)}{E}\frac{\partial^2 u_r^{\text{thin}}}{\partial t^2} = 0.\end{aligned} \tag{14}$$

Equilibrium in the tangential direction provides the following:

$$\begin{aligned}&\frac{1}{a}\frac{\partial^2 u_\theta^{\text{thin}}}{\partial \theta^2} - \frac{1}{a}\frac{\partial u_r^{\text{thin}}}{\partial \theta} + a\frac{\left(1 - \nu^2\right)}{Eh}\tau_{r\theta}^{\text{thin}} \\ &\quad - \rho a \frac{\left(1 - \nu^2\right)}{E}\frac{\partial^2 u_\theta^{\text{thin}}}{\partial t^2} = 0,\end{aligned} \tag{15}$$

where a is the radius of the metro segment, h is the thickness of the metro segment, ρ is the density of metro segment material, and E and ν are Young's modulus and Poisson's ratio of

the segment material, respectively. The effects of the material damping on system vibration in the frequency domain are considered by adopting composite material parameters. The time domain dynamic loading is converted into the frequency domain using a Fast Fourier Transform expressed as $\widetilde{\sigma}_r^{\text{thin}}$ and $\widetilde{\tau}_{r\theta}^{\text{thin}}$.

Assuming that the load applied is harmonic in the time domain, the stress can be expressed by

$$\begin{aligned} \sigma_r^{\text{thin}}(\theta,t) &= \widetilde{\sigma}_r^{\text{thin}} \cos n\theta e^{i\omega t} \\ \tau_{r\theta}^{\text{thin}}(\theta,t) &= \widetilde{\tau}_{r\theta}^{\text{thin}} \sin n\theta e^{i\omega t}. \end{aligned} \tag{16}$$

With reference to formula (16), the harmonic displacements equation, which satisfies (14) and (15), can be expressed as follows:

$$\begin{aligned} u_r^{\text{thin}}(t) &= \widetilde{u}_r^{\text{thin}} \cos n\theta e^{i\omega t} \\ u_\theta^{\text{thin}}(t) &= \widetilde{u}_\theta^{\text{thin}} \sin n\theta e^{i\omega t}, \end{aligned} \tag{17}$$

where n is an integer number of waves developed around the circumference, ω is the frequency, and the tilde on $\widetilde{\sigma}_r^{\text{thin}}$ and $\widetilde{\tau}_{r\theta}^{\text{thin}}$ or $\widetilde{u}_r^{\text{thin}}$ and $\widetilde{u}_\theta^{\text{thin}}$ indicates stresses or displacements in the frequency field, respectively.

Substituting the stress (16) and displacement (17) into the vibration balance (14)-(15) develops the general solution of the metro segment in the frequency domain:

$$[A]\begin{Bmatrix} \widetilde{u}_r^{\text{thin}} \\ \widetilde{u}_\theta^{\text{thin}} \end{Bmatrix} = \frac{-a\left(1-\nu^2\right)}{Eh}\begin{Bmatrix} \widetilde{\sigma}_r^{\text{thin}} \\ \widetilde{\tau}_{r\theta}^{\text{thin}} \end{Bmatrix}. \tag{18}$$

The displacements $\widetilde{u}_r^{\text{thin}}$ and $\widetilde{u}_\theta^{\text{thin}}$ are based on the mode number n and are calculated with the applied stress in the frequency field. The total displacement is obtained through linear superposition from the calculation results of each modal number.

3.2. A Segment-Soil Interaction Model with the Elastic Continuum Theory. The segment-soil interaction model is established to describe a tunnel surrounded by soil, as shown in Figure 4. The segment structure is considered as a liner-elastic material. The surrounding soil is a saturated, homogeneous, isotropic elastic solid, and the range of the soil in the space extends infinitely. The coordinate, displacement, and stress directions are shown in Figure 4.

The wave equation describing motion is derived by Watson [34]:

$$\mu\nabla^2 u + (\lambda+\mu)\nabla\nabla u + \rho p = \rho\frac{\partial^2 u}{\partial t^2}, \tag{19}$$

where ∇ is the Laplace operator, u is the displacement vector, t is time, ρ is the density of the medium, and λ and μ are the Lamé constants of the bulk material: $\lambda = 2\nu G/(1-2\nu)$ and $\mu = E/2(\nu+1) = G$, where G is the shear modulus, E is Young's modulus, and ν is Poisson's ratio. Equation (19) represents an elastic, isotropic, and homogeneous medium. This paper

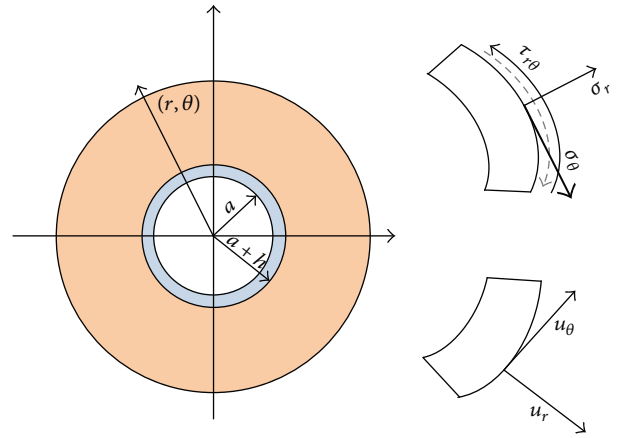

Figure 4: A soil elastic continuum model.

mainly studies the vibration about the equilibrium position; therefore, the body forces P are set to zero.

The displacement equation (19) is satisfied when the values satisfy the following [35]:

$$\nabla^2\phi = \frac{1}{c_1^2}\frac{\partial^2\phi}{\partial t^2}, \tag{20}$$

where c_1 is the pressure wave velocity in the medium and $c_1 = \sqrt{(\lambda+2\mu)/\rho}$.

The Laplacian in (20) is given by the following equation [34]:

$$\nabla^2\phi = \frac{1}{r}\frac{\partial\phi}{\partial r} + \frac{\partial^2\phi}{\partial r^2} + \frac{1}{r^2}\frac{\partial^2\phi}{\partial\theta^2}. \tag{21}$$

In (19), the components of the displacement u under a cylindrical coordinate system are as follows:

$$\begin{aligned} u_r &= \frac{\partial\phi}{\partial r}, \\ u_\theta &= \frac{1}{r}\frac{\partial\phi}{\partial\theta}. \end{aligned} \tag{22}$$

The geometric equations of the soil bulk are as follows:

$$\begin{aligned} \varepsilon_{rr} &= \frac{\partial u_r}{\partial r}, \\ \varepsilon_{\theta\theta} &= \frac{1}{r}\frac{\partial u_\theta}{\partial\theta} + \frac{u_r}{r} \\ \varepsilon_{r\theta} &= \frac{1}{2}\left(\frac{1}{r}\frac{\partial u_r}{\partial\theta} + \frac{\partial u_\theta}{\partial r} - \frac{u_\theta}{r}\right). \end{aligned} \tag{23}$$

The soil damping ratio only minimally affects the vibration amplitudes in the vibration model. Additionally, limited energy is caused by the small-amplitude vibration of the soil when the vibration energy transfers from the rail to the sleeper, to the ballast bed, to the segment, and then to the soil. This analysis assumes that the soil is a linear elastic material and Hooke's law is valid for this material.

The constitutive equation of the soil is as follows:

$$\begin{bmatrix} \sigma_r \\ \sigma_\theta \\ \tau_{r\theta} \end{bmatrix} = \begin{bmatrix} \lambda + 2\mu & \lambda & 0 \\ \lambda & \lambda + 2\mu & 0 \\ 0 & 0 & 2\mu \end{bmatrix} \begin{bmatrix} \varepsilon_{rr} \\ \varepsilon_{\theta\theta} \\ \varepsilon_{r\theta} \end{bmatrix}. \tag{24}$$

The displacements and the stress components can be solved using (19)–(24). The scalar wave potential specifying the radial variation of the potentials that describe the displacements can be assumed in the following form:

$$\phi = f(r) \cos n\theta e^{i\omega t}, \tag{25}$$

where n is the vibration modal number of tunnel segments, reflecting the shell vibration deformation. By substituting (24) into (20) and combining with (21), the governing equation is obtained as follows:

$$r^2 f'' + rf' - \left[n^2 - \frac{\omega^2}{c_1^2} r^2 \right] f = 0. \tag{26}$$

Equation (26) is a modified Bessel equation of order n and can be solved based on the solution of the modified Bessel equation of order n. The solution of the transformed equation for f is as follows:

$$f = AI_n(\alpha r) + BK_n(\alpha r), \tag{27}$$

where A and B are arbitrary constants determined by the boundary conditions, respectively, I_n and K_n are the modified Bessel functions of the first and second type of order n, respectively, and $\alpha^2 = -\omega^2/c_1^2$ and $\beta^2 = -\omega^2/c_2^2$, in which c_1 and c_2 are the pressure wave velocity and shear wave velocity in the medium, respectively, and $c_2 = \sqrt{\mu/\rho}$.

Substituting (27) and (25) into (22), the displacement and stress of each part in the system can be solved. The displacements in the radial direction and tangential direction can be expressed as follows:

$$\begin{aligned} u_r &= f' \cos n\theta e^{i\omega t}, \\ u_\theta &= -\frac{n}{r} f \sin n\theta e^{i\omega t}. \end{aligned} \tag{28}$$

The stress can be expressed as follows:

$$\begin{aligned} \sigma_r &= \left[(\lambda + 2\mu) f'' + \frac{\lambda}{r} f' - \lambda \left(\frac{n^2}{r^2} \right) f \right] \cos n\theta e^{i\omega t} \\ \sigma_\theta &= \left[\lambda f'' + \frac{(\lambda + 2\mu)}{r} f' - (\lambda + 2\mu) \left(\frac{n^2}{r^2} \right) f \right] \\ &\quad \cdot \cos n\theta e^{i\omega t} \\ \tau_{r\theta} &= \left[-2\mu \frac{n}{r} f' + 2\mu \frac{n}{r^2} f \right] \sin n\theta e^{i\omega t}. \end{aligned} \tag{29}$$

The harmonic displacements and the stress of the model can be expressed in terms of the matrix form as follows:

$$\begin{aligned} u &= \begin{Bmatrix} u_r \\ u_\theta \end{Bmatrix} = \begin{bmatrix} \cos n\theta & 0 \\ 0 & \sin n\theta \end{bmatrix} \cdot [U] \cdot C e^{i\omega t} \\ \tau &= \begin{Bmatrix} \sigma_r \\ \tau_{r\theta} \\ \sigma_\theta \end{Bmatrix} = \begin{bmatrix} \cos n\theta & 0 & 0 \\ 0 & \sin n\theta & 0 \\ 0 & 0 & \cos n\theta \end{bmatrix} \cdot [T] \cdot C e^{i\omega t}. \end{aligned} \tag{30}$$

In the matrix, $C = \{A \;\; B\}^T$ is the vector of coefficients determined by the boundary conditions, ω is the angular frequency, n is the circumferential modal number, and r is the radius of the tunnel segment.

Correspondingly, the harmonic solutions for the stress equation and displacement equation are determined through the Laplace transform. In the frequency domain, the solution of the stress and displacement is shown as

$$\begin{aligned} \begin{Bmatrix} \widetilde{u}_{rn} \\ \widetilde{u}_{\theta n} \end{Bmatrix} &= [U] \cdot C \\ \begin{Bmatrix} \widetilde{\sigma}_{rn} \\ \widetilde{\sigma}_{\theta n} \end{Bmatrix} &= [T] \cdot C. \end{aligned} \tag{31}$$

In the process of composing the metro segment-soil interaction model, the tunnel segment in the soil adopts a liner-elastic thin circle, and the soil adopts an elastic continuum surrounding the tunnel.

To solve the model, three boundary conditions are required [35]:

(1) Soil displacement and tunnel segment displacement are synchronized in the contact face, and the dynamic stress is in equilibrium at the interface of the tunnel segment and soil.

(2) The stress in the bottom of the tunnel segment equals the applied loading, and the corresponding position on the outside of the tunnel is not arranged with the force.

(3) The soil extends along the radius to infinity, and the soil displacement at the infinite attenuation is set to zero.

According to the second assumption, (18) can be written as follows:

$$\begin{aligned} [A_E] \cdot \widetilde{U}_n &= \frac{-Eh}{a(1 - \nu^2)} [A] \begin{Bmatrix} \widetilde{u}_r \\ \widetilde{u}_\theta \end{Bmatrix} = \begin{Bmatrix} \widetilde{Q}_{rn} \\ \widetilde{Q}_{\theta n} \end{Bmatrix} \\ &= \begin{Bmatrix} \widetilde{P}_{rn} \\ \widetilde{P}_{\theta n} \end{Bmatrix} - \begin{Bmatrix} \widetilde{\sigma}_r^{\text{thin}} \\ \widetilde{t}_{r\theta}^{\text{thin}} \end{Bmatrix}_{\text{outside}}. \end{aligned} \tag{32}$$

The third assumption can be used to reduce the dimensions of the continuum vibration response equations. In the solution for the stresses and displacements of the soil expressed in (30), the modified Bessel functions $I_n(\alpha r)$,

$K_n(\alpha r)$, $I_n(\beta r)$, and $K_n(\beta r)$ were originally used as solutions for the function f in (27). Where $\alpha^2 = -\omega^2/c_1^2$ and $\beta^2 = -\omega^2/c_2^2$, when the radius $|r| \to \infty$, $|\alpha r| \to \infty$, $|\beta r| \to \infty$, and $K_n(\infty)$ tends to zero without a limit, whereas $I_n(\infty)$ increases [36]. Therefore, the solution can satisfy only boundary condition three when $A \cdot I_n(\infty) = 0$, indicating the following:

$$A = 0 \Longrightarrow C = \{0 \;\; B\}^T. \tag{33}$$

In (30), matrices $[U]$ and $[T]$ (which are formed by the modified Bessel functions) can neglect I_n from the matrix. Therefore, the computational time is reduced in half. Correspondingly, the Bessel equations I_n and I_{n+1} included in matrices $[U]$ and $[T]$ can be removed from the matrix, and the amount of computational time is again reduced in half.

A dynamic system model is established by coupling the tunnel shell and soil. However, the coordinate systems used in the two models are different, and the conversion formulas for the stresses and displacements are as follows:

$$\begin{aligned} u_\theta{}^{\text{thin}} &\equiv u_\theta, \\ \tau_{r\theta}{}^{\text{thin}} &\equiv -\tau_{r\theta}, \\ u_r{}^{\text{thin}} &\equiv -u_r, \\ \sigma_r{}^{\text{thin}} &\equiv \sigma_r. \end{aligned} \tag{34}$$

The displacement equations at the tunnel-soil interface are as follows:

$$\begin{aligned} \begin{Bmatrix} \widetilde{u}_r{}^{\text{thin}} \\ \widetilde{u}_\theta{}^{\text{thin}} \end{Bmatrix} &= \begin{Bmatrix} -\widetilde{u}_{rn} \\ \widetilde{u}_{\theta n} \end{Bmatrix}_{r=a} = \begin{bmatrix} -u_{12} \\ u_{22} \end{bmatrix}_{r=a} \cdot B \\ &= [U_\infty]_{r=a} \cdot B. \end{aligned} \tag{35}$$

The stress equations at the interface of the shell and the soil are as follows:

$$\begin{aligned} \begin{Bmatrix} \widetilde{\sigma}_r{}^{\text{thin}} \\ \widetilde{\tau}_{r\theta}{}^{\text{thin}} \end{Bmatrix}_{\text{outside}} &= \begin{Bmatrix} \widetilde{\sigma}_r \\ -\widetilde{\tau}_{r\theta} \end{Bmatrix}_{r=a} = \begin{bmatrix} t_{12} \\ -t_{22} \end{bmatrix}_{r=a} \cdot B \\ &= [T_\infty]_{r=a} \cdot B, \end{aligned} \tag{36}$$

where u_{12}, u_{22}, t_{12}, and t_{22} are components of the U and T matrix. The loading size of the segment external surface can be determined by substituting (36) into (32). Using (35), the displacement of the model and corresponding specific numerical solution for the parameters could be obtained. By sorting the above formula, the following formula can be expressed:

$$\begin{Bmatrix} \widetilde{U}_n \\ B \end{Bmatrix} = \begin{bmatrix} [A_E] & [T_\infty]_{r=a} \\ [I] & -[U_\infty]_{r=a} \end{bmatrix}^{-1} \begin{Bmatrix} \widetilde{P}_n \\ 0 \end{Bmatrix}, \tag{37}$$

where $[I]$ is a $2 * 2$ identity matrix. The displacements $\widetilde{U}_n = \{\widetilde{u}_r{}^{\text{thin}} \;\; \widetilde{u}_\theta{}^{\text{thin}}\}^T$ at the surface of the tunnel segment and soil can be obtained through (37), and P_n is the load calculated in Section 2. $\widetilde{P}_n$ can be determined through a fast discrete Fourier transformation (DFT) from the load P_n. The displacements anywhere (r, θ) in the soil away from the center of the tunnel circle can be calculated from the following equation:

$$\widetilde{U}_n\big|_{r,\theta} = [U_\infty]_{r,\theta} \cdot B. \tag{38}$$

However, the displacements calculated above target a particular modal number n, and the total displacements can be determined by superimposing enough modal displacement components in the frequency domain.

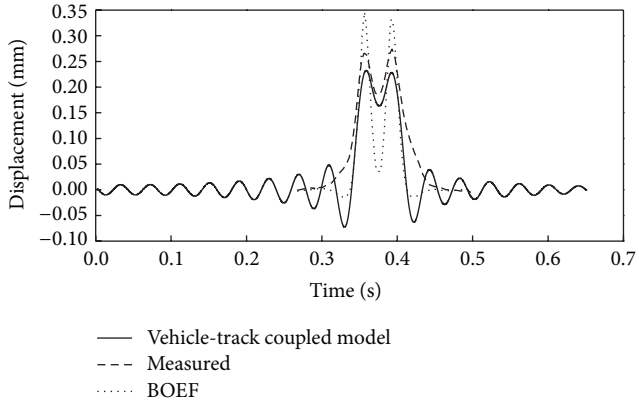

Figure 5: Comparison of the measured sleeper displacement with that obtained from the vehicle-track coupled model and the BOEF model for a single bogie.

4. Analysis of the Results

4.1. The Load Calculated by the Excitation Model for the Vehicle-Track Vibration. The speed of the metro vehicle is 40–80 km/h, and the faster the speed, the larger the wheel-track contact force. In this calculation, the speed of the vehicle is set to 80 km/h. According to the vehicle-track nonlinear coupled model shown in Section 2 and the values of the parameters shown in Tables 1 and 2, the displacement of the sleeper can be determined with the Newmark integration method. Priest and Powrie [37] used geophones to measure the displacement of the sleeper during train service and a modified beam in the elastic foundation method (BOEF) to calculate the displacement of the sleeper. The time domain result is shown in Figure 5.

A similar behavior in the sleeper displacement during operation is shown in Figure 5. The results from the vehicle-track coupled model are closer to the measured values than with the BOEF method; however, the decay of the displacement is slower than in the BOEF method because of the modal analysis.

The full vehicle model is necessary when analyzing the settlement of the tunnel because the length of the vehicle can affect the frequency of the tunnel displacement. The Nanjing subway marshals six cars to the trains. The establishment of the full vehicle model is similar to a single bogie model

Table 1: Vehicle parameters.

Quantity	Car body quality (M_c)	Bogie quality (M_t)	Bogie nod inertia (J_t)	Wheel quality (M_w)	Primary suspension stiffness (K_{sz})	Primary suspension damping (C_{sz})	The second suspension stiffness (K_{pz})	The second suspension damping (C_{pz})	Half of bogie wheelbase (l_h)
Value	38500 Kg	2980 kg	3605 kg/m^2	1350 kg	2.14×10^6 N/m	4.9×10^4 N·s/m	2.535×10^6 N/m	1.96×10^5 N·s/m	1.2 m

Table 2: Wheel coupling system orbit parameters.

Quantity	The quality of the rail unit length (M_r)	Rail elastic modulus (E)	Rail section inertia (I)	Fastener vertical stiffness (K_r)	Fastener damping (C_r)	Sleeper quality (m_s)
Value	60 kg/m	2.059×10^{11} Pa	2.037×10^{-5} m^4	7.8×10^7 N/m	5×10^4 N·s/m	125 kg
Quantity	The sleeper spacing (a)	Under the sleeper rubber pad stiffness (K_s)	Under the sleeper rubber pad damping (C_s)	C40 concrete elastic modulus (E_c)	Concrete Poisson's ratio (ν)	
Value	0.545 m	7.8×10^7 N/m	5.88×10^4 N·s/m	3×10^{10} Pa	0.2	

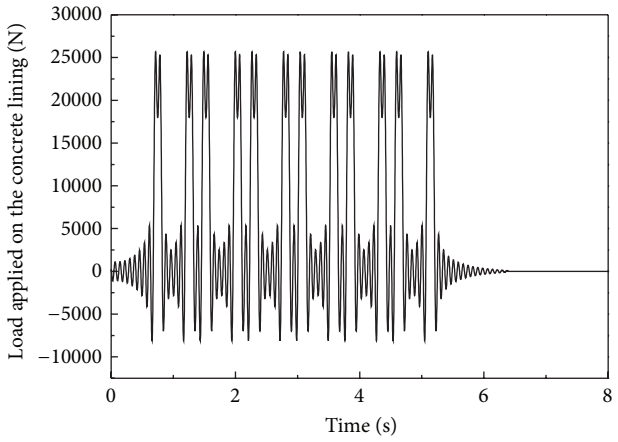

Figure 6: Vertical load applied on the tunnel shell.

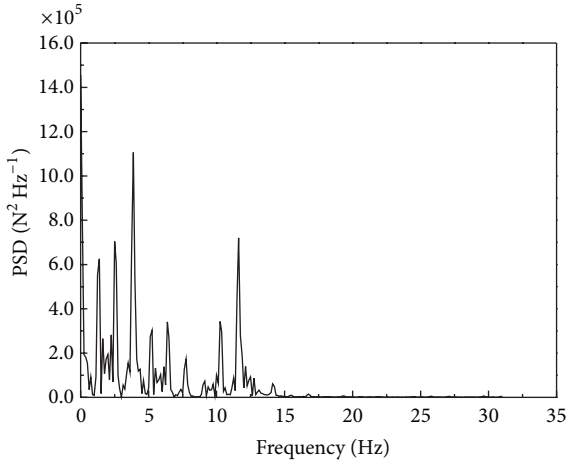

Figure 7: PSD of the load applied on the tunnel shell in the frequency domain.

but must consider only the nod inertia of the train. The magnitude of the vertical load on tunnel shell at 80 km/h can be calculated according to (39), and the result is shown in Figure 6. Consider

$$P = Z_b K_b + V_b C_b. \tag{39}$$

The main frequency range of the load frequency spectra for a single bogie is 0–30 Hz (Figure 7). Because of the damping of the fasteners and the rubber boots, the high frequency wheel-track contact force only minimally affects the load applied on the tunnel shell.

4.2. Calculation of the Total Displacement of the Tunnel. The total displacement of the tunnel can be calculated by substituting the load obtained in Section 4.1 using the segment-soil interaction coupled model. The calculation parameters for the segments in the model are shown in Table 3.

Samples of the soft soil in Nanjing of China were collected by a thin-wall soil sampler. The sampler is cylindrical with a height of 30 cm and diameter of 11 cm as shown in Figure 8. The dynamic triaxial tests are conducted by the GDS system

Figure 8: Cylindrical samples.

shown in Figure 9. The GDS dynamic triaxial system can monitor in real-time during tests. Therefore, test data can be recorded and accessed in high speed. The calculation parameters of the soft soil for the segment-soil interaction coupled model are measured under cyclic load of 75 kpa, 1 Hz

Table 3: The parameters for the tunnel segments.

Quantity	Young's modulus (E)	Poisson's ratio (ν)	Density (ρ)	Pressure wave velocity (c_1)	Shear wave velocity (c_2)	Inner diameter (a)	Thickness of the tunnel shell (h)
Value	3.45×10^{10} Pa	0.17	2450 Kg/m^3	5189 m/s	2774 m/s	2.7 m	30 m

Table 4: The parameters of the soil.

Quantity	Young's modulus (E)	Poisson's ratio (ν)	Density (ρ)	Pressure wave velocity (c_1)	Shear wave velocity (c_2)
Value	6×10^6 Pa	0.3	1859 Kg/m^3	524 m/s	190 m/s
Quantity	Lamé elastic constants (λ)	Lamé elastic constants (μ)	Bulk modulus (K)	Volumetric damping (η_K)	Hysteretic loss factor (η_G)
Value	1.4×10^9 Pa	1.91×10^8 Pa	1.528×10^9 Pa	0	0.06

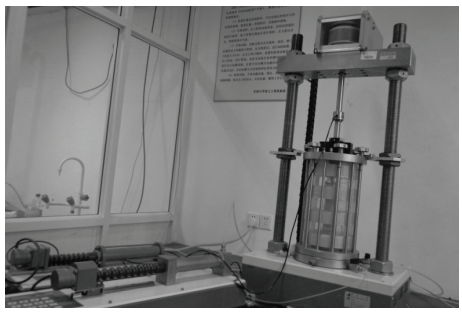

Figure 9: GDS test system.

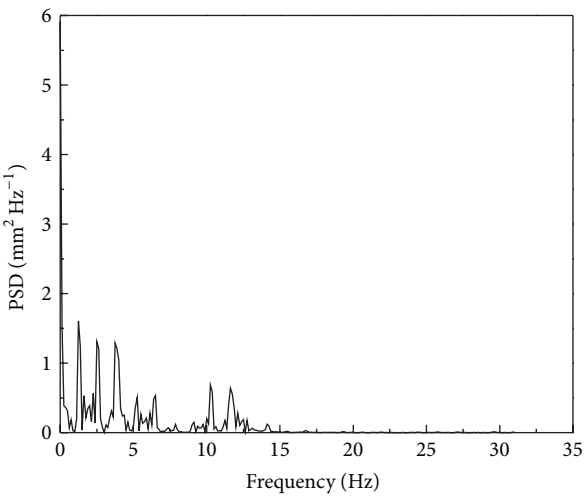

Figure 10: PSD of the displacement at the shell-soil contacting position in the frequency domain.

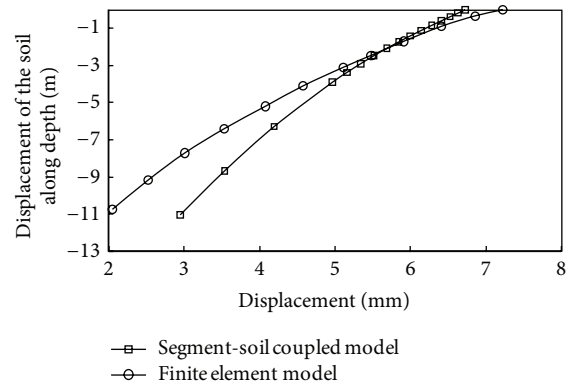

Figure 11: Settlement along the depth of the soil.

frequency, and 5000 load cycles; the specific values of the parameters are shown in Table 4.

The total displacement of the tunnel segments and the location of the soil are obtained by superposing every model displacement. The soil displacement response under every model number is calculated by substituting the parameters values shown in Tables 1 and 2 combined with the load calculated in the vehicle-track coupled model.

Figure 10 shows the soil displacement frequency spectra response at the concrete tunnel shell-soft soil contacting position of the load applied to the tunnel. At a lower frequency, three crests at approximately 2, 3, and 4 Hz are observed, approximately the applied load frequency spectra. At 10 and 12 Hz, the applied load frequency spectra display obvious crests, but this response of the displacement frequency spectra is rapidly attenuated with the increase in frequency. This attenuation is likely because of the energy absorption by the rigid tunnel lining and the radiation damping by the infinite soft soil surrounding the tunnel.

The distribution of the settlement of the tunnel over time can be obtained by the inverse Fourier transform through Figure 10, drawing the curve of the maximum settlement along the depth of the model as shown in Figure 11. The layered settlement of the soil decreases with increasing the depth of the incensement parting from the tunnel segment shown in Figure 11. The depth of the soil reduced from 0 m to 11 m. The settlement of the tunnel reduced from 6.72 mm to 2.94 mm, and the speed of the subsidence decreased with increasing depth. The vibration energy decreases because of soil damping, and the compactness of the soil decreases with increasing depth. Therefore, the settlement value nearly exponentially decays. Figure 11 shows that the settlement of the soil calculated by the finite element model is larger at the contact position of the soil and tunnel lining than the calculated results from the segment-soil interaction

coupled model. This higher value is likely because of the elastic deformation and plastic deformation of the soil in this position occurring simultaneously under the action of the finite element model is based on the Mohr-Coulomb elastic-plastic element. The subsidence decreases rapidly with increasing depth, mainly because the plastic deformation absorbs vibrational energy when transferred in the soil. For the subway tunnel, the main effect of the soil deformation occurs from 0 to 3 meters, and the calculated results of the settlement were similar to the settlement values from two types of models in this range. The results also illustrate that the segment-soil interaction coupled model calculation value can respond to the settlement of the metro tunnel during train operation.

5. Conclusions

The settlement behaviors of a metro tunnel in Nanjing city of China are investigated in this paper. The following conclusions can be drawn from this study:

(1) The excitation model for the vehicle-track vibration and a segment-soil interaction coupled model for the infinite radial extent are established in this study. The sleeper displacement of the metro tunnel can be calculated using the vehicle-track coupled model. The calculation results show the accuracy of this method compared with the BOEF method and this method agrees with the measured sleeper vertical displacements.

(2) The applied load caused by the train operation at the bottom of the tunnel is calculated by the vehicle-track model, and substitute the load in the frequency domain into the segment-soil model to obtain the displacement of any position in the soil.

(3) The position of the crests of the displacement frequency spectra is near the load frequency spectra applied on the tunnel segment; however, this value decays rapidly with increasing frequencies. The analytical inversion of the Fourier transformation with respect to frequency leads to numerical solutions for the displacements in the soft soil area, and the displacements along the vertical direction are obtained. The displacement of the soil below the tunnel reduced from 7.27 mm to 0.91 mm as the depth increased from 0 m to 35 m; the reduction curve was nearly exponential.

Conflict of Interests

The authors declare that there is no conflict of interests regarding the publication of this paper.

Acknowledgments

This work was supported by the National Natural Science Foundation of China (no. 51278099). The authors thank the reviewers for their valuable comments.

References

[1] T. YiQun, Z. Hua, W. YuanDong et al., "Characteristics of strain accumulation of reinforced soft clay around tunnel under subway vibration loading," *Journal of Tongji University. Natural Science*, vol. 39, no. 7, pp. 972–977, 2011.

[2] S. Timoshenko, "Method of analysis of statical and dynamical stresses in rail," in *Proceedings of the 2nd International Congress of Applied Mechanics*, pp. 12–17, Zurich, Switzerland, 1926.

[3] H. A. Dieterman and A. Metrikine, "Critical velocities of a harmonic load moving uniformly along an elastic layer," *Journal of Applied Mechanics*, vol. 64, no. 3, pp. 596–600, 1997.

[4] T. K. Caughey and M. E. O'Kelly, "Effect of damping on the natural frequencies of linear dynamic systems," *The Journal of the Acoustical Society of America*, vol. 33, pp. 1458–1461, 1961.

[5] S. D. Garvey, M. I. Friswell, and U. Prells, "Co-ordinate transformations for second order systems. Part I: general transformations," *Journal of Sound and Vibration*, vol. 258, no. 5, pp. 885–909, 2002.

[6] S. L. Grassie, R. W. Gregory, D. Harrison et al., "The dynamic-response of railway track tohigh-frequency vertical excitation," *Journal of Mechanical Engineer Science*, vol. 24, no. 2, pp. 77–90, 1982.

[7] W. Zhai, K. Wang, and C. Cai, "Fundamentals of vehicle-track coupled dynamics," *Vehicle System Dynamics*, vol. 47, no. 11, pp. 1349–1376, 2009.

[8] X. Lei and N.-A. Noda, "Analyses of dynamic response of vehicle and track coupling system with random irregularity of track vertical profile," *Journal of Sound and Vibration*, vol. 258, no. 1, pp. 147–165, 2002.

[9] J. C. O. Nielsen and A. Igeland, "Vertical dynamic interaction between train and track influence of wheel and track imperfections," *Journal of Sound and Vibration*, vol. 187, no. 5, pp. 825–839, 1995.

[10] B. Ripke and K. Knothe, "Simulation of high frequency vehicle-track interactions," *Vehicle System Dynamics*, vol. 24, supplement 1, pp. 72–85, 1995.

[11] Y. Q. Sun and M. Dhanasekar, "A dynamic model for the vertical interaction of the rail track and wagon system," *International Journal of Solids and Structures*, vol. 39, no. 5, pp. 1337–1359, 2002.

[12] R. D. Fröhling, "Low frequency dynamic vehicle/track interaction: modelling and simulation," *Vehicle System Dynamics*, vol. 29, supplement 1, pp. 30–46, 1998.

[13] H. E. M. Hunt, "Modelling of rail vehicles and track for calculation of ground-vibration transmission into buildings," *Journal of Sound and Vibration*, vol. 193, no. 1, pp. 185–194, 1996.

[14] T. Balendra, C. G. Koh, and Y. C. Ho, "Dynamic response of buildings due to trains in underground tunnels," *Earthquake Engineering & Structural Dynamics*, vol. 20, no. 3, pp. 275–291, 1991.

[15] V. Krylov and C. Ferguson, "Calculation of low-frequency ground vibrations from railway trains," *Applied Acoustics*, vol. 42, no. 3, pp. 199–213, 1994.

[16] J. A. Forrest and H. E. M. Hunt, "A three-dimensional tunnel model for calculation of train-induced ground vibration," *Journal of Sound and Vibration*, vol. 294, no. 4, pp. 678–705, 2006.

[17] A. V. Metrikine and A. C. W. M. Vrouwenvelder, "Surface ground vibration due to a moving train in a tunnel: two-dimensional model," *Journal of Sound and Vibration*, vol. 234, no. 1, pp. 43–66, 2000.

[18] W. Gardien and H. G. Stuit, "Modelling of soil vibrations from railway tunnels," *Journal of Sound and Vibration*, vol. 267, no. 3, pp. 605–619, 2003.

[19] T. Ekevid, H. Lane, and N.-E. Wiberg, "Adaptive solid wave propagation—Influences of boundary conditions in high-speed train applications," *Computer Methods in Applied Mechanics and Engineering*, vol. 195, no. 4–6, pp. 236–250, 2006.

[20] S.-H. Ju, "Finite element investigation of traffic induced vibrations," *Journal of Sound and Vibration*, vol. 321, no. 3–5, pp. 837–853, 2009.

[21] K. Vogiatzis, "Environmental ground borne noise and vibration protection of sensitive cultural receptors along the Athens Metro Extension to Piraeus," *Science of the Total Environment*, vol. 439, pp. 230–237, 2012.

[22] F. Guan and I. D. Moore, "Three-dimensional dynamic response of twin cavities due to travelling loads," *Journal of Engineering Mechanics*, vol. 120, no. 3, pp. 637–651, 1994.

[23] S. A. Kostarev, "An analysis of vibrational field, generated by an underground tunnel in soil," *Journal of Low Frequency Noise & Vibration*, vol. 15, no. 4, pp. 151–156, 1996.

[24] J. E. Snyder III and D. N. Wormley, "Dynamic interactions between vehicles and elevated, flexible randomly irregular guideways," *Transactions of the ASME—Journal of Dynamic Systems, Measurement and Control*, vol. 99, no. 1, pp. 23–33, 1977.

[25] S. G. Newton and R. A. Clark, "An investigation into the dynamic effects on the track of wheelflats on railway vehicles," *Journal of Mechanical Engineering Science*, vol. 21, no. 4, pp. 287–297, 1979.

[26] S. Timoshenko, *Vibration Problems in Engineering*, John Wiley & Sons, 4th edition, 1974.

[27] S. Zhu, J. Lou, and Q. He, *Vibration Theory and Vibration Isolation Technology*, National Defense Industry Press, 2006.

[28] Z. Y. Shen, J. K. Hedrick, and J. A. Elkins, "A comparison of alternative creep force models for rail vehicle dynamic analysis," *Vehicle System Dynamics*, vol. 12, no. 1–3, pp. 79–78, 1983.

[29] W.-M. Zhai, "Two simple fast integration methods for large-scale dynamic problems in engineering," *International Journal for Numerical Methods in Engineering*, vol. 39, no. 24, pp. 4199–4214, 1996.

[30] L. Andersen and C. J. C. Jones, "Coupled boundary and finite element analysis of vibration from railway tunnels—a comparison of two- and three-dimensional models," *Journal of Sound and Vibration*, vol. 293, no. 3–5, pp. 611–625, 2006.

[31] B. Jin, Z. Q. Yue, and L. G. Tham, "Stresses and excess pore pressure induced in saturated poroelastic halfspace by moving line load," *Soil Dynamics and Earthquake Engineering*, vol. 24, no. 1, pp. 25–33, 2004.

[32] B. Jin, "Dynamic displacements of an infinite beam on a poroelastic half space due to a moving oscillating load," *Archive of Applied Mechanics*, vol. 74, no. 3-4, pp. 277–287, 2004.

[33] R. K. N. D. Rajapakse, "Stress analysis of borehole in poroelastic medium," *Journal of Engineering Mechanics*, vol. 119, no. 6, pp. 1205–1226, 1993.

[34] G. N. Watson, *A Treatise on the Theory of Bessel Functions*, Cambridge University Press, 1995.

[35] K. F. Graff, *Wave Motion in Elastic Solids*, Courier Dover Publications, 1975.

[36] M. Abramowitz, *Handbook of Mathematical Functions*, Dover, New York, NY, USA, 1972.

[37] J. A. Priest and W. Powrie, "Determination of dynamic track modulus from measurement of track velocity during train passage," *Journal of Geotechnical and Geoenvironmental Engineering*, vol. 135, no. 11, pp. 1732–1740, 2009.

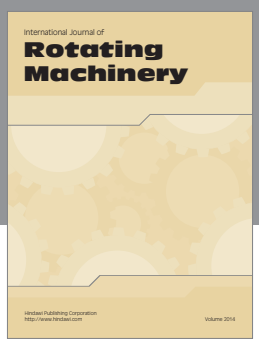

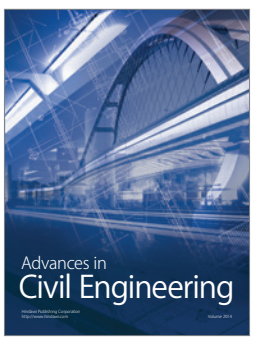

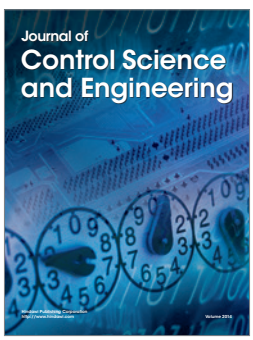

Hindawi
Submit your manuscripts at
http://www.hindawi.com